Biosensors and Bioelectronics 265 (2024) 116696

Contents lists available at ScienceDirect

Biosensors and Bioelectronics

journal homepage: www.elsevier.com/locate/bios

Multifunctional Tetrode-like Drug delivery, Optical stimulation, and Electrophysiology (Tetro-DOpE) probes

Jongwoon Kim [a], Earl Gilbert [b], Kaiser Arndt [b], Hengji Huang [a], Patrycja Oleniacz [d], Shan Jiang [d], Ian Kimbrough [d], Harald Sontheimer [d], Daniel Fine English [b,**], Xiaoting Jia [a,b,c,*]

[a] The Bradley Department of Electrical and Computer Engineering, Virginia Tech, Blacksburg, VA, USA
[b] School of Neuroscience, Virginia Tech, Blacksburg, VA, USA
[c] Department of Materials Science and Engineering, Virginia Tech, Blacksburg, VA, USA
[d] Department of Neuroscience, School of Medicine, University of Virginia, Charlottesville, VA, USA

A B S T R A C T

Having reliable tools for recording and manipulating circuit activity are essential to understand the complex patterns of neural dynamics that underlie brain function. We present Tetro-DOpE (Tetrode-like Drug delivery, Optical stimulation, and Electrophysiology) probes that can simultaneously record and manipulate neural activity in behaving rodents. We fabricated thin multifunctional fibers (<50 μm) using the scalable convergence thermal drawing process. Then, the thin fibers are bundled, similar to tetrode fabrication, to produce Tetro-DOpE probes. We demonstrated the multifunctionality (i.e., electrophysiology, optical stimulation, and drug delivery) of our probe in head-fixed behaving mice. Furthermore, we assembled a six-shank probe mounted on a microdrive which enabled stable recordings of over months when chronically implanted in freely behaving mice. These *in vivo* experiments demonstrate the potential of customizable, low cost, and accessible multifunctional Tetro-DOpE probes for investigation of neural circuitry in behaving animals.

1. Introduction

Understanding how neural activity encodes information on a systems level requires studying neural spiking and circuit activity in awake and behaving animals (Buzsáki, 2004; Carandini, 2012; Wang, 2010; Buzsáki and Draguhn, 2004; Rubin et al., 2019; Yuste et al., 2005; Ekstrom et al., 2003). Tools that enable monitoring single neuron action potentials in behaving animals have yielded some of the most striking discoveries of the neural correlates of behavior (e.g. place cells using single wires and grid cells using tetrodes) (Hafting et al., 2005; O'Keefe and Dostrovsky, 1971; Hong et al., 2019; Schultz, 1986; Bruce et al., 1981). Tetrodes are used widely by the neuroscience community due to low-cost of fabrication, ease of adapting the probes in new experimental designs and the ability to perform single-unit isolation in anatomically dense neuronal populations (e.g. pyramidal layer of the hippocampus) (Hafting et al., 2005; Gray et al., 1995; Mokri et al., 2017). Such classical tetrodes are passive recording devices, that is they cannot modulate neural activity. Leveraging advances in fluorescent protein sensors and optogenetics (Emiliani et al., 2022; Deisseroth, 2015; Joshi et al., 2020; Chen et al., 2022; Fenno et al., 2011; Wang et al., 2023; Ovechkina et al., 2021), bi-directional neural probes have been developed allowing simultaneous monitoring and manipulation of neural activity via electrodes and light delivery (Eunah et al., 2022; Zhao et al., 2017; Rubehn et al., 2013; Zou et al., 2021; Kim et al., 2020; Zhou et al., 2022). More recently, multifunctional probes with additional manipulation dimensions, such as drug delivery channels, have emerged (Jiang et al., 2020; Kim et al., 2024; Jeong et al., 2015; Shin et al., 2019; Yoon et al., 2022). Developing multifunctional "tetrode"-like neural probes that harness the advantages of tetrodes while also enabling simultaneous multimodal neural modulation would open new avenues of systems neuroscience investigation.

There has been significant progress in multifunctional neural probes over the past few years (Zou et al., 2021; Shin et al., 2015; Garwood et al.; Vöröslakos et al., 2022; Ouyang et al., 2023). However, existing multifunctional probes have a fixed configuration once fabricated, and it is difficult to customize the probes for different applications. In addition, most of the multifunctional probes are fabricated using cleanroom microfabrication techniques which are time consuming and expensive. Alternatively, the thermal drawing process (TDP) has been developed as a promising platform for producing low cost and scalable multifunctional neural probes (Jiang et al., 2020; Kim et al., 2024; Garwood et al.; Sahasrabudhe, 2023; Zheng et al., 2023; Park et al., 2017; Canales et al.,

* Corresponding author. The Bradley Department of Electrical and Computer Engineering, Virginia Tech, Blacksburg, VA, USA.
** Corresponding author.
E-mail addresses: neurodan83@vt.edu (D.F. English), xjia@vt.edu (X. Jia).

https://doi.org/10.1016/j.bios.2024.116696
Received 9 April 2024; Received in revised form 21 August 2024; Accepted 21 August 2024
Available online 23 August 2024

2015). The process was originally adapted from optical fiber fabrication, where glass preforms (macro version of fiber) are heated and pulled to thin fibers. The TDP process enables scalable fabrication of multi-material (i.e., metal, polymer, semiconductor) fiber via optimization of furnace temperature and fiber pulling speed. The fiber is cut into segments and assembled into fiber-based sensors and actuators. However, there are two major challenges with this technology: (1) similar to other multifunctional probes, a new probe configuration would require a separate thermal drawing process from a new preform. (2) To achieve a small sensing end, the backend necessarily decreases in size (due to the uniform diameter along the fiber length), making the connection process harder and more complicated.

To overcome these challenges, we implemented a bundling process, similar to the preparation of classical tetrodes, into our device fabrication. In this work, the bundling process refers to a method of assembling thin thermally drawn multifunctional fibers (~50 μm) together. We fabricated various designs of thin multifunctional fibers that can be bundled in any combination using the thermal drawing process. Unlike conventional probe fabrication processes, in which once the device is designed, the fabricated batch of device design cannot be altered, this bundling process allows for rapid in-house customization of the device configuration, meaning that we can easily change the device design by choosing different types and counts of the thin functional fibers to form the bundle. Due to the relatively low count of features (electrodes, optical waveguide, and microfluidic channel) in each thin fiber, connection to the outside modules (recording setups, lasers, and microfluidic pumps) is a trivial process. As a result, we developed a fabrication method where the thin multifunctional fibers are bundled to produce tetrode-like drug delivery, optical stimulation, and electrophysiology (Tetro-DOpE) probes (Fig. 1).

Here, we present highly customizable and affordable Tetro-DOpE probes which enable simultaneous electrophysiology recording, optogenetic manipulations, and local drug infusion. We designed various thin multifunctional fibers via the scalable convergence thermal drawing process which are then bundled to fabricate Tetro-DOpE probes. To demonstrate recording quality, probes were implanted in hippocampus CA1 and reliably recorded canonical CA1 circuit dynamics including theta oscillations and sharp wave-ripples (SPW-Rs) without inducing pathological states (e.g. seizures). We verified the functional ability for optical waveguides and microfluidic channels to manipulate neuronal activity in head-fixed behaving mice. To illustrate the high customizability of Tetro-DOpE probes, we assembled six-shank probes on a microdrive. The assembled probes were chronically implanted bilaterally in dorsal CA1, and stable long-term recordings were obtained in such freely moving mice. These *in vivo* experiments demonstrate that our highly scalable and customizable Tetro-DOpE probes are capable of reliably recording and manipulating neural activity in freely behaving animals.

2. Results

2.1. Tetro-DOpE fabrication via thermal drawing process

Various designs of Tetro-DOpE probes were assembled by bundling thin multifunctional polymer fibers (<50 μm), fabricated using the convergence thermal drawing process (CTDP (Fig. 2a)). Critically, CTDP enables the fabrication of fibers composed of multiple materials, even those with vastly different thermal properties such as metals and thermoplastics (i.e., tungsten wire and polycarbonate (PC) preform). This process was previously established by Rein et al., in 2018 (Rein et al., 2018). Here, we demonstrate the utilization of CTDP for fabricating metal wires as thin as 15 μm in diameter, suitable for tetro-DOpE probe production. First, we used machining techniques to fabricate macro designed preforms consisting of a PC core (refractive index = 1.59), polyvinylidene fluoride (PVDF) cladding (refractive index n = 1.41), and one or two hollow channels for the insertion of tungsten metal electrodes. Then, the preform is further wrapped in PC film, a sacrificial layer that stabilizes the drawing process and thermally consolidated (Supplementary Fig. 1). The preform was mounted in a custom-built furnace, heated, and pulled while tungsten wires (15 μm) were simultaneously fed into the hollow channels. The sacrificial PC layer is chemically etched with Dichloromethane (DCM) reducing the fiber diameter to <50 μm. The optical waveguide is composed of the PC core and PVDF cladding with a reported transmission (a.u.) of 0.9–1 at a wavelength from 500 to 900 nm[29], while convergence of the tungsten wires within the empty channels results in functional electrodes. Three different fiber designs are illustrated in Fig. 2b: one electrode and one optical waveguide (F1), two electrodes and one optical waveguide (F2), and one electrode and one microfluidic channel (F3). The fibers produced with CTDP are flexible enough to be wrapped around a human finger without damage (Fig. 2c), and hundreds of meters can be fabricated from a single CTDP draw. Here, we provide a guideline for

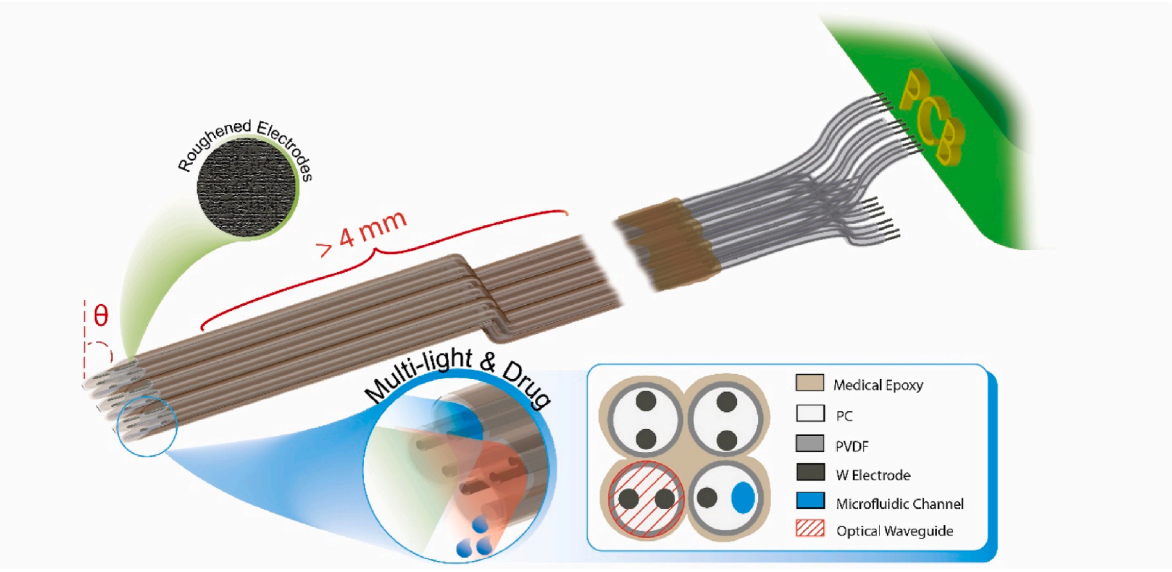

Fig. 1. Illustration of the Tetro-DOpE probe. The probe enables multi-light and drug delivery. These bundled probes can be further assembled into bulks and/or shanks to increase the feature counts (i.e., electrodes, channels, and optical waveguides).

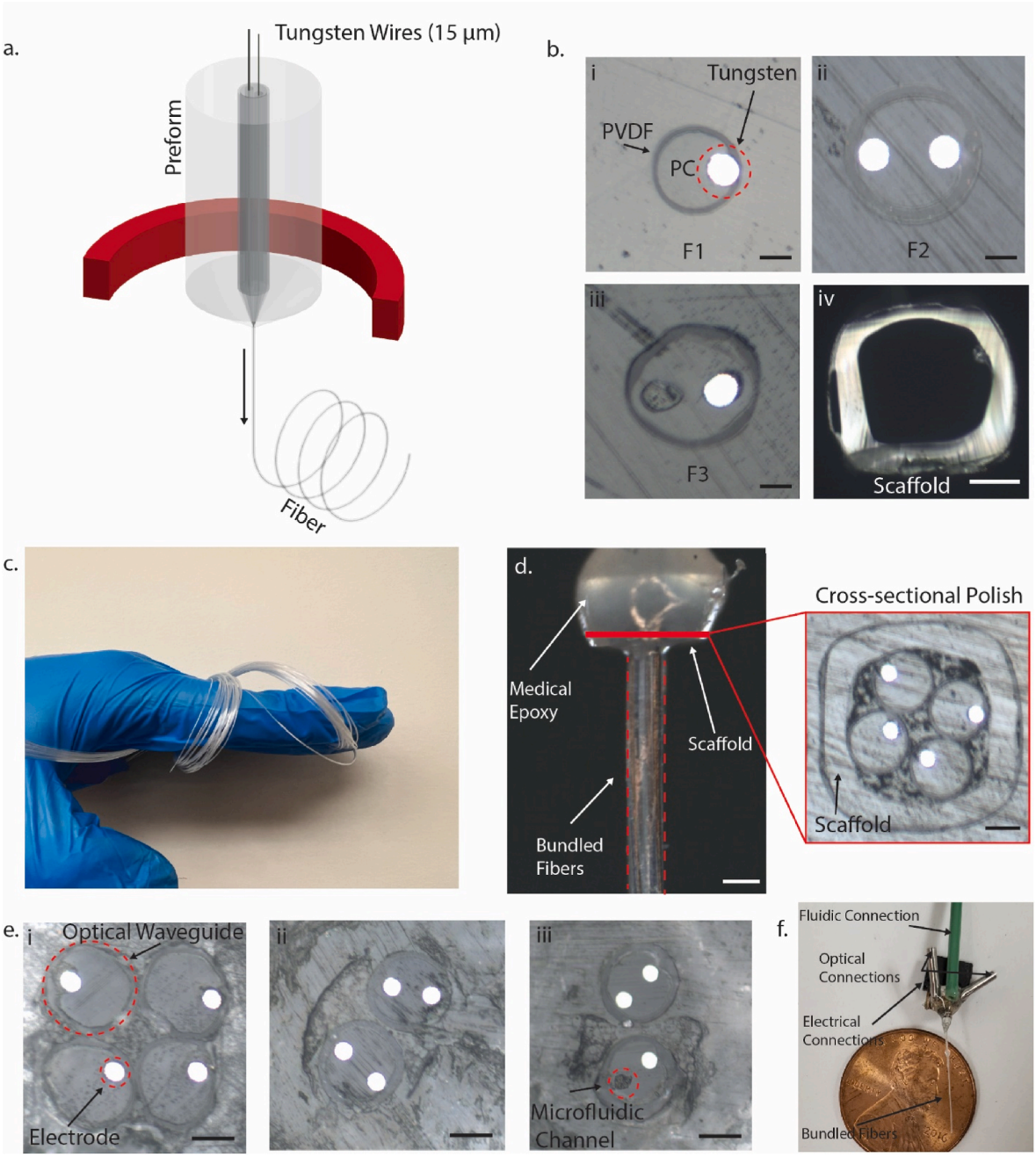

Fig. 2. **a.** Schematic of the convergence thermal drawing process. **b.** Thermally drawn fiber with various designs before chemically etched. (i. one electrode and one waveguide (Scale bar: 15 μm). ii. two electrodes and one waveguide (Scale bar: 15 μm). iii. one electrode and one channel (Scale bar: 15 μm). iv. Scaffold (Scale bar: 30 μm)) **c.** Demonstration of the flexibility and the scalability of the fibers. **d.** Enlarged photograph and cross-sectional image of the scaffold and bundled fibers. The sliding scaffold cleans the excess medical epoxy. (Scale bar: 100 μm, 30 μm) **e.** Cross-sectional image of the Tetro-DOpE probes with various configurations. (i. four electrodes and four waveguides. ii. four electrodes and two waveguides. iii. Three electrodes, one waveguide, and one channel) (Scale bar: 30 μm) **f.** Image of a working probe connected to fluidic tube, optical ferrules, and pin connectors.

bundling thin multifunctional fibers to fabricate Tetro-DOpE probes. The step-by-step illustration is provided in the Supplementary Fig. 2. First, the electrodes, optical waveguides, and/or microfluidic channels of the multifunctional fibers are connected to copper wires, optical ferrules, and/or fluidic tubes (back-end connection). Second, the fully connected thin fibers are threaded into a short PC scaffold under a microscope, arranging the fibers into a tetrode configuration (Fig. 2d). Third, the bundled fibers are coated with a thin layer of medical epoxy while undergoing small tension to keep the bundle straight. Next, the PC scaffold slides along the fiber length to remove excess medical epoxy. Lastly, the sensing tip of the bundled fibers are polished at an angle using a polishing station. One key advantage of the bundling process is that the back-end connection does not require scraping. Scraping is a process of exposing electrodes by peeling off the insulating material layer by layer using a knife under a microscope, and then using conductive paste and metal wires to connect the electrodes to external circuits. This process is time-consuming and labor-intensive, which significantly limits the number of electrodes connectable in thermally drawn neural fiber probes. Due the low count of electrodes in the thin multifunctional fiber, the electrodes can be directly soldered to the copper wires, without scraping. The overall diameter of device is roughly 100 μm in diameter. The fiber in our manuscript refers to the individual fibers and the overall

bundle is referred to as the device. Various designs of Tetro-DOpE probes are shown in Fig. 2e: (i) four electrodes and four optical waveguides, (ii) four electrodes and two optical waveguides, and (iii) three electrodes, two optical waveguides, and one microfluidic channel. Illustrated in Fig. 2f is a fully assembled Tetro-DOpE probe with three electrodes for electrophysiology, two optical waveguides for optogenetics, and one microfluidic channel for local pharmacological intervention.

2.2. Tetro-DOpE probe characterization

Due to the small cross sectional area of the tungsten electrode (diameter: 15 μm), the impedance of the electrodes at 1 kHz is ~ 1MΩ. Although action potentials can be reliably recorded with this impedance range, (Neto et al., 2018) larger surface area increases the double layer capacitance and improves the charge transfer at the interface, which reduces the impedance of the electrode and also increases the signal to noise ratio (Ahmed and Reifsnider, 2011). Overall, this leads to a better spike sorting quality. To decrease impedance, we increased the surface area by roughening the electrode surface with silicon carbide polishing film. The cross-sectional image of the polished and roughened electrodes are shown in Fig. 3a along with the respective spectral impedance measurement. Surface roughening decreased impedance more than two-fold (from ~1.1 MΩ–0.4MΩ). To demonstrate the flexibility of the fibers, we measured the bending stiffness of thin fibers with one electrode (15 μm tungsten wire, overall diameter 50 μm; F1) and fibers with two electrodes (two 15 μm tungsten wire, overall diameter 50 μm; F2) using a dynamic mechanical analyzer. The fiber design F2 has higher bending stiffness than fiber design F1 due to additional tungsten

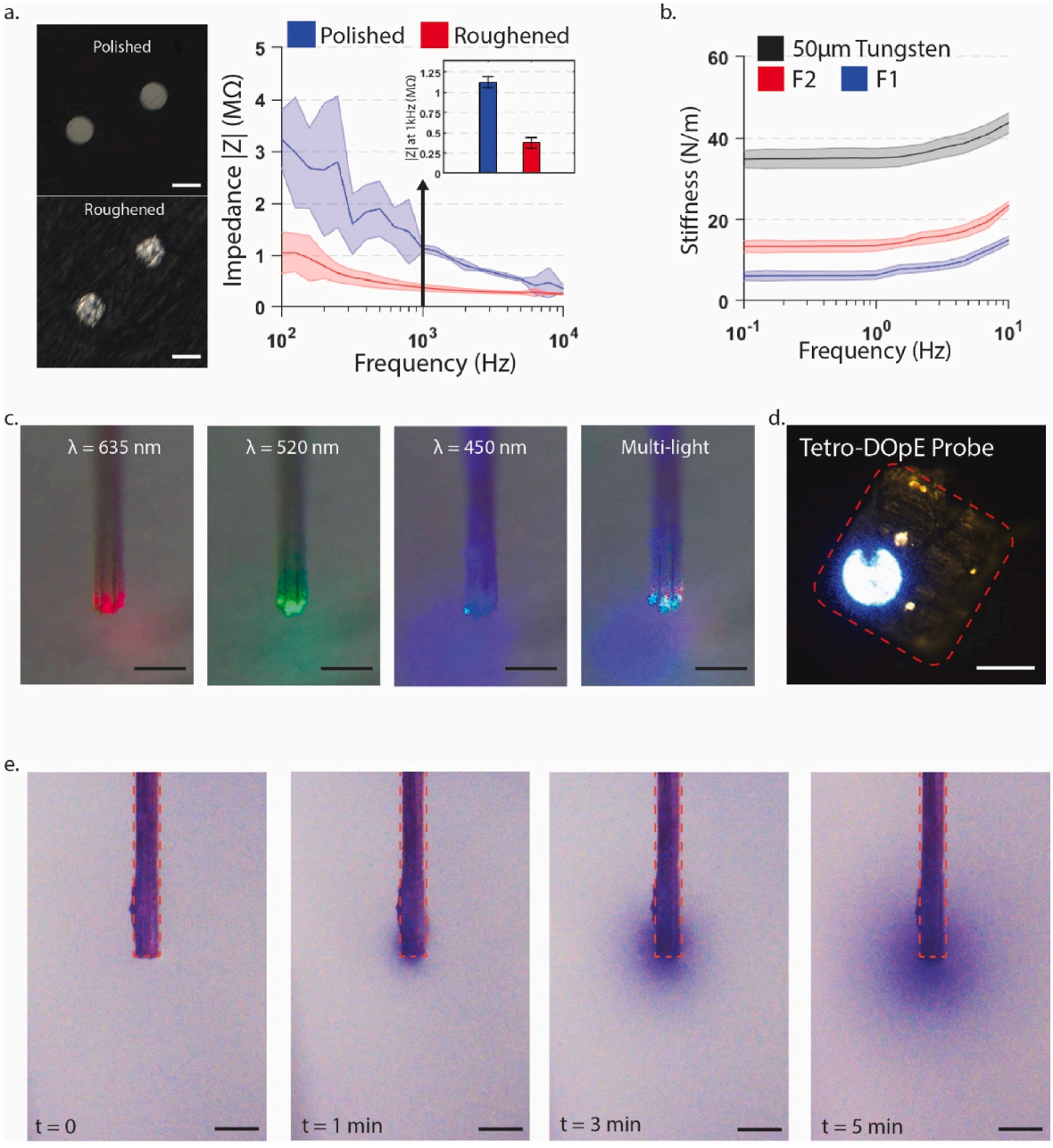

Fig. 3. a. Impedance measurement of polished and roughened electrodes. (Scale bar: 15 μm) **b.** Bending stiffness of fiber design F1 and F2 compared with 50 μm tungsten wire. **c.** Demonstration of individually addressable optical waveguide (Scale bar: 200 μm) **d.** Cross-sectional image of the probe with the optical stimulation. (Scale bar: 50 μm) **e.** Time-lapsed images to demonstrate the drug infusion using a food coloring at 1 nL/s infusion rate in a 0.6% agarose gel phantom. (Scale bar: 200 μm).

electrodes, which are the least flexible component (i.e., F2 has two electrodes while F1 has one electrode). To characterize the bending stiffness of our probe, we calculated the bending stiffness by computing 3EI/L3, where E is the Young's Modulus of the material, I is the second moment of inertia, which is a function of the cross-section, and L is the length of the beam. We calculated an effective second moment of inertia that is 3.5–16 times larger with respect to different probe designs. The expected bending stiffness of the probes are 59.5–80 N/m, which is comparable to a 50 μm tungsten wire. To demonstrate the optical delivery capability, a Tetro-DOpE device with the design in Fig. 2c (ii) (four electrodes and four optical waveguides) were connected to diode-pumped solid-state (DPSS) lasers with various wavelengths (λ = 635 nm, 520 nm, 450 nm) commonly used in optogenetics. Fig. 3c are images from the time-lapse video (supplementary video 1) demonstrating the individual addressability of the optical waveguides. The light transmission is well confined within the optical waveguides as shown in Fig. 3d. Furthermore, we inserted our Tetro-DOpE probe in 0.6% agarose gel and infused purple food coloring dye to demonstrate drug delivery capability via the microfluidic channel. Dye was diffused into the agarose gel phantom during 5 min of dye infusion through the

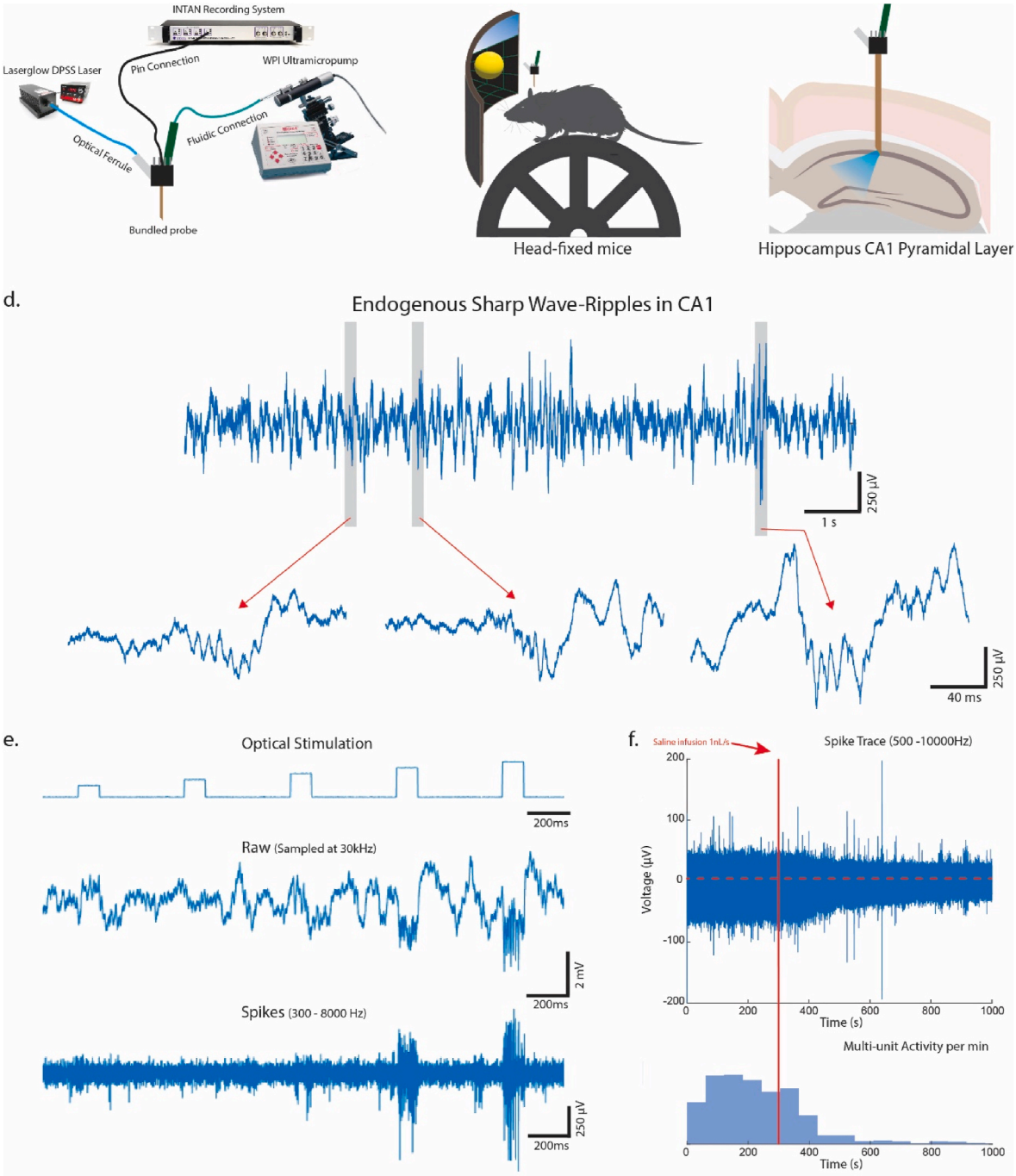

Fig. 4. **a.** Hardware equipment used in the tri-modality *in-vivo* setup. **b.** Illustration of the mouse setup. A head-fixed, wild-type mouse is mounted on the wheel. A virtual reality environment is presented on the screen to instigate running. **c.** Schematic of the targeted implant site, hippocampus CA1. **d.** Example wideband (0.1–8000 Hz) extracellular trace from CA1 recorded using Tetro-DOpE probe. The trace shows three different instances of sharp wave-ripple. **e.** Raw and filtered traces of optically evoked neural responses at various optical stimulation power. Note the different neural responses at single-unit resolution and group depolarization with respect to different optical powers. **f.** Physical cell displacement due to focal saline infusion.

channel (Fig. 3e). These results demonstrate functional performance of Tetro-DOpE probes.

2.3. In-vivo validation of Tetro-DOpE probes

To evaluate *in vivo* function we used tungsten electrodes to obtain electrophysiological recordings using the electrodes, optogenetically manipulated neural circuitry with the optical waveguides, and infused saline using the microfluidic channel. The Tetro-DOpE probes are connected to an Intan recording system using the pin connections, to DPSS laser using optical ferrules and silica fibers, and to WPI micropumps using fluidic connection (Fig. 4a). An illustration of the experimental set-up is shown in Fig. 4b with mice running on a wheel in 1-D virtual reality, promoting spontaneous running behavior. The probe implantation was targeted to the hippocampus CA1 pyramidal cell layer (Fig. 4c). Fig. 4d shows an example wideband extracellular recording (0.1–8000 Hz) in the CA1 of hippocampus. Within the 10-s-window, we observed three individual sharp wave-ripples (SPW-Rs; 150–250 Hz oscillation lasting 50–100 ms), a reliable electroanatomical landmark suggesting proximity to the pyramidal layer of hippocampus CA1 (Wilson et al., 1994; Buzsáki, 2015a; Buzsáki et al., 1983). Additionally, multi-unit activity (population spiking) is clearly present in the raw trace (Fig. 4d). By reliably implanting and recording from the targeted region across animals (CA1, n = 8 animals), we demonstrate that our Tetro-DOpE probe can record both multi-unit activity and local field potentials without disrupting the local circuitry. Furthermore, we expressed Channelrhodopsin-2 (ChR2) in CA1 pyramidal cells to validate the optical waveguides in the Tetro-DopE probes. CA1 was optically stimulated at five intensities. Optically evoked changes in neural activity were observed as negative deflections and oscillations in the raw LFP and increased spiking in the 0.3–8 kHz band pass filtered signal Fig. 4e. The resolution of optical stimulation enables reliable optical induction of SPW-Rs without generating higher-frequency pathological oscillations (Supplementary Fig. 3). (Stark et al., 2014; Kovács et al., 2016; Buzsáki, 2015b; Fernández-Ruiz, 2019; Zutshi and Buzsáki, 2023; Zhang et al., 2021; Liu et al., 2022) We further optically stimulated to demonstrate populational neural activation under 4 Hz optogenetic stimulation (Supplementary Fig. 4). Note that at lower optical power, population depolarization is not visible (multi-unit activity shown in Supplementary Fig. 5). With these optogenetic experiments (animal number = 4), we demonstrate a high sensitivity in the optogenetic stimulation using our Tetro-DOpE probes. To evaluate the local infusion via the microfluidic channel, we infused 200 nL of saline with a rate of 1 nL/s. As expected, we observed a silence in the spike trace after saline infusion (Fig. 4f), which is explained by the physical displacement of the cells (Kim et al., 2024; Yoon et al., 2022; Shin et al., 2015). Altogether, we successfully demonstrated the *in vivo* functionalities (electrophysiology, optical stimulation, and local infusion) of our novel Tetro-DOpE probes.

2.4. High customizability of Tetro-DOpE probes

Unlike the existing multifunctional probes, the Tetro-DOpE probes can easily increase the feature counts by bundling more fibers (Supplementary Fig. 6) or be assembled in specific configurations for the user's need. To illustrate the high customizability of the Tetro-DOpE probe, we adapted the conventional shank configurations of the silicon probes. As shown in Fig. 5a, the shank configured Tetro-DOpE probes were mounted on a 3-D printed plate with a microdrive (Vöröslakos et al., 2021) and implanted into the hippocampus CA1 in both side of the hemispheres. The three shanks in each hemisphere are 150 μm apart from one another. Each shank has four electrodes. A photograph of the probes epoxied onto the 3-D printed plate is shown in Fig. 5b. Unlike the silicon probe, the configuration of these shanks can easily be altered via changing the geometry of the 3-D printed plate. For the first time, we reliably recorded with thermally drawn fiber-based probe with 24 electrode sites in a freely moving chronic mouse (Fig. 5c). Fig. 5d shows chronic, raw recording at the electrode sites. We clustered the action potentials using a combination of waveform template and principal component analysis (PCA). From the multi-unit (population activity) we were able to sort a high firing rate CA1 interneuron, shown in Fig. 5e. The respective auto-correlogram is plotted in Fig. 5f. The PCA of the multi-unit and interneuron clusters are shown in Fig. 5g. Altogether, the high customizability of the configurations provides a high flexibility in recording sites for future investigation of cross brain regions.

2.5. Fiber biocompatibility

Reactive tissue response to our multifunctional probe was assessed using immunohistochemical analysis of surrounding brain tissue from mice implanted for two weeks with either a multifunctional probe or a conventional stainless-steel wire with a diameter of 125 μm. The presence of glial fibrillary acidic protein (GFAP) was used to assess astrocyte reactivity to the probe, ionized calcium-binding adaptor molecule 1 (Iba1) was used as a marker of microglial response, and lastly, the neuron-specific protein NeuN was used to analyze neuronal density. Representative images from the multifunctional probe and stainless-steel probe are presented in Fig. 6. Neuronal density, microglia density, and astrocyte reactivity were compared between all groups, and no significant difference was observed, Fig. 6e–g. Furthermore, we computed the Root Mean Square (RMS) of the neural signal chronically recorded from the freely behaving mouse, provided in the Supplementary Table 1. We concluded with the immunohistochemistry comparison and the electrophysiology analysis that our probe is stable and biocompatible for chronic investigations.

3. Discussion

Here, we fabricated Tetro-DOpE probes by bundling thin multifunctional fibers produced with scalable and low-cost convergence thermal drawing process. The low count of features (i.e., electrodes, optical waveguides, and microfluidic channels) in each fiber enables simple connection to the outside module (i.e., pins, PCBs, ferrules, and tubes). The Tetro-DOpE probes reliably record *in vivo* electrophysiology (i.e., LFP and multi-unit activity), while enabling focal light and drug delivery. We assembled a six-shank Tetro-DOpE device with recording and optical stimulation capabilities to demonstrate the customizability of the probe. The device was mounted on a microdrive and implanted into the hippocampus, enabling bilateral CA1 recording in freely moving mice.

For most fiber-based neural probes, there is a trade-off between the ease of back-end connection and the density of electrodes, optical waveguides, and microfluidic channels. Using the traditional scraping method, the back-end connection gets substantially harder with higher counts of electrodes and optical waveguides in a single device. In our prior work, (Kim et al., 2024) we overcame this challenge by implementing a tapering process, where we created a tapered device with a thick backend for facile connection (2 mm in diameter) and a small tip (<150 μm) for neural interfacing. In this work, we adapt the bundling process to overcome the trade-off. Each fiber in the bundle consists of only one or two electrodes, and one optical waveguide or microfluidic channel, which enables easy and fast connection. The time-consuming and labor-intensive scraping process is no longer needed, replaced by direct soldering for electrical connection. As a result, we fabricated fiber-based devices with higher counts of features, while maintaining the ease of connection by bundling thin multifunctional fibers (<50 μm). The convergence thermal drawing process produces hundreds of meters of these thin multifunctional fibers which can easily be distributed like the insulated wires used for classic tetrode preparation. The material cost of the thin multifunctional fibers is < $2 per meter and could be lowered in industrial operation settings. Any academic laboratory would

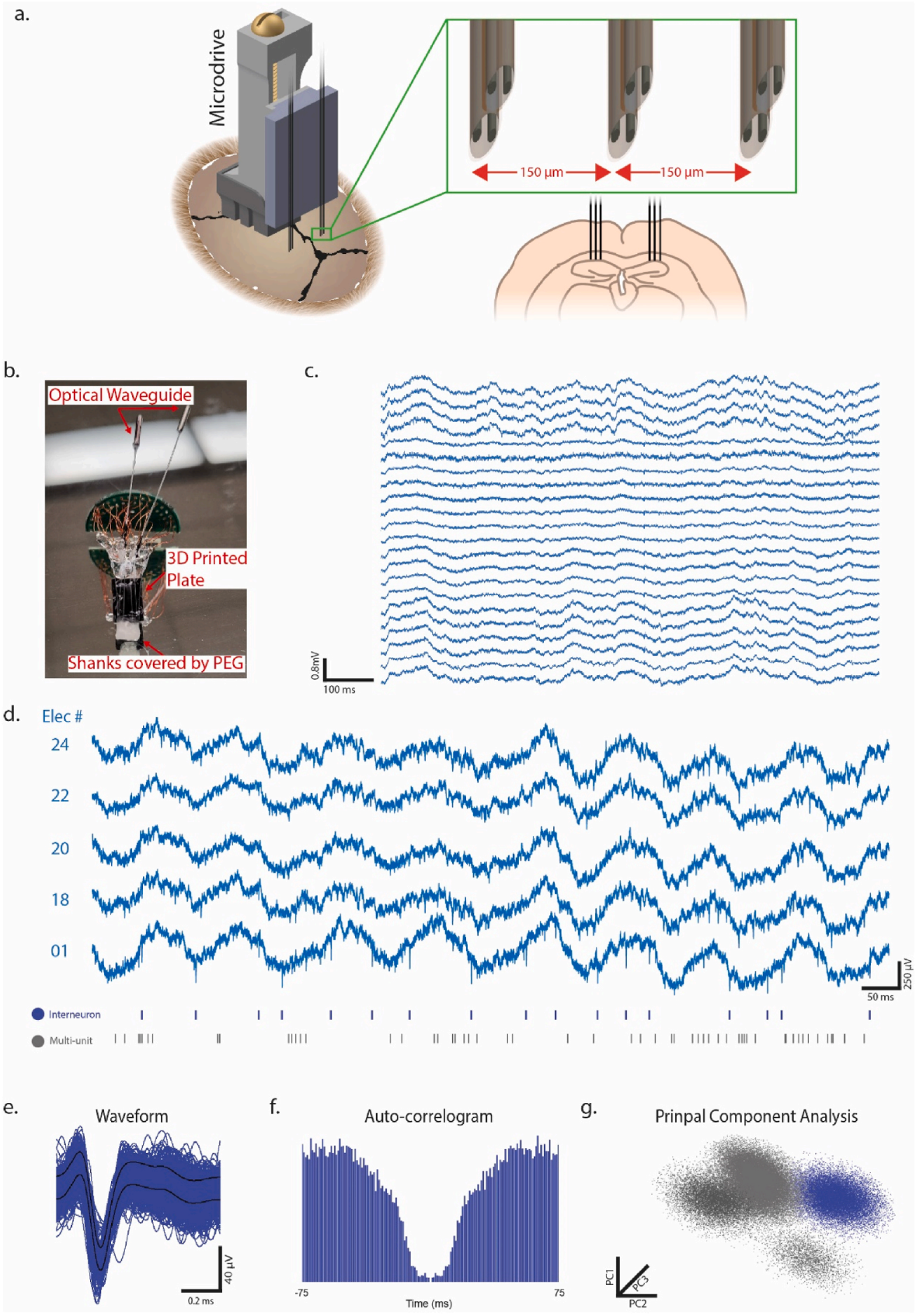

Fig. 5. a. Schematic of the experimental set up. The Tetro-DOpE probes were assembled into shanks enabling bilateral recording of hippocampus CA1. The assembled probes were mounted onto the microdrive, which is 3d printed with aluminum. **b.** Photograph of the assembled probes with the PCB, optical ferrules, and 3-D printed plate. c. A representative recording from 24 electrodes. **d.** Raw recording at different electrode sites from a freely moving chronic mouse implanted with

the Tetro-DOpE probe. **e.** waveforms and the standard deviation of the identified unit. **f.** Auto-correlogram of the identified unit. **g.** Principal component analysis of the units.

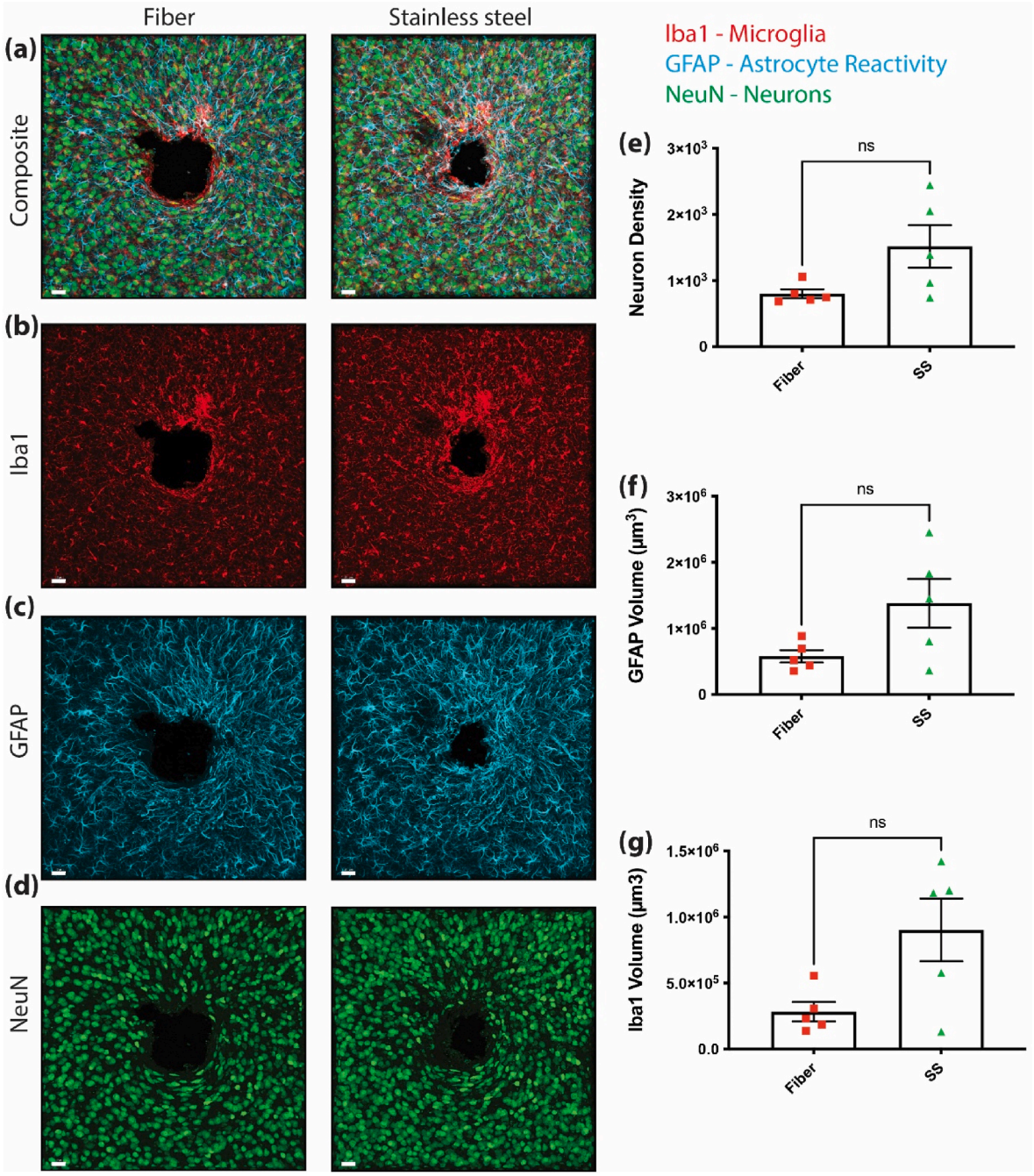

Fig. 6. Immunohistochemical comparison of tissue reaction to chronically implanted fibers (Left) and conventional stainless-steel probes (Right) after two-week implantation. (a–d). Confocal Z-stacks through a volume of 19.5 μm at 650 nm intervals were taken at the electrode implantation site. Neurons were labeled with NeuN (green), astrocytes with GFAP (cyan), and microglia with Iba1 (Red). (d,e) Neuron density, calculated by counting NeuN labeled neurons, was not significantly different between the groups. (c,f) Astrocyte and microglia (b,g) reactivity, measured as the volume of GFAP- or Iba1-positive cells respectively, was not significantly different between groups. Significance was determined by Welch's student's t-test. Error bars on bar graphs reflect the standard error of the mean. (Scale bar: 30 μm)

be able to connect the features of the probes and bundle the thin fibers to make a Tetro-DOpE probe, just like a traditional tetrode. Altogether, we present flexible, customizable, low cost, and accessible Tetro-DOpE probes.

4. Method

4.1. Preform fabrication

Preform is the macroscale version of the fiber. The possible materials of multifunctional polymer probes largely consist of thermoplastics,

metal, and semi crystalline. All polymer materials (films, tubes, and rods) were baked in 80 °*C* vacuum oven to ensure no water molecules reside within the polymer. Three various fibers were drawn for this study. However, the second and third design are the same except that there exists an electrode instead of the microfluidic channel. Since this difference will be accounted in the thermal drawing process, we only designed and fabricated two preforms. For the first design, a PC rod (McMaster-Carr) is milled for the wire to be inserted into during the CTDP. The milled rode is rolled with PC films (Laminated Plastics) and then with PVDF films (McMaster-Carr). After PVDF films, we roll another layer of PC films. The rolled preform is consolidated in a vacuum oven at 190 °C. During this process, the films consolidate to form a hard PC and PVDF matrix without any gaps (Supplementary Fig. 1). For the second design, the procedure is similar to that of the first design except for an additional mill on the other side of the PC rod. The milled PC rod is then rolled with PC films and PVDF films and consolidated.

4.2. Thermal drawing process

Thermal drawing process requires a specialized thermal draw tower. The preform is mounted onto the preform holder and fed into a custom-built furnace which has three temperature zones. The top zone preheats the preform, the middle zone softens the preform, and the last zone cools down the fiber. After the preform has softened in the middle zone, the bottom of the preform is pulled down via a capstan motor at a controlled manner to fabricate the fiber. The feeding speed of the preform and the pulling speed of the fiber along with the temperature of the furnace controls the final geometry of the fiber. The three temperature zones of the furnace were set to 150 °C, 275 °C and 120 °C respectively. The middle zone temperature, feeding speed and pulling speed were closely controlled to keep the fiber (PC scaffold) at 300 μm.

Convergence thermal drawing process enables multi-material fiber drawing with vastly different thermal behavior. While the fiber is drawn, materials can be fed into the empty channel and clamped. For our fiber design 1 and 2, we used our first and second design of preform respectively. We fed in 15um tungsten wire (Midwest Tungsten) as the fiber is being drawn. For the fiber design 3, we leave one channel empty, which becomes the microfluidic channel and feed tungsten wire on the other empty channel.

4.3. Device fabrication

The outer PC cladding for the fiber is chemically etched with DCM. Fiber is then cut into ~5 cm segments and connected with corresponding modules (i.e., electrodes to insulated copper wires, optical waveguide to optical ferrules, and microfluidic channel to non-elastic tubing). Then, four fully connected fibers are fit into ~3 mm scaffold in a 2 × 2 structure. The top of the bundle structure is glued together with an optical resin. Then, the scaffold slides down holding the bundle fiber in a 2 × 2 with some tension. The overall bundle is applied with medical epoxy and the scaffold slides up and down to remove excess medical epoxy. After the medical epoxy cures, the top of the bundle is cut with a razor blade and polished and roughened using a polishing station (Krelltech) at an angle. The copper wires are then connected to either pin connectors or a PCB.

4.4. Electrochemical spectral impedance measurement

Impedance measurements were collected via a potentiostat (Gamry Instruments). The measurements were gathered by lowering the sensing end of a fully connected Tetro-DOpE probe into phosphate-buffered saline (PBS, Thermo Fisher). A platinum wire (Basi) was used for a counter and the reference electrode. Finally, we used the Gamry's proprietary software to forward the spectral impedance data.

4.5. Headbar implantation

Mice, mounted in a stereotax, are induced, and maintained at a surgical plane of anesthesia with isoflurane. Hair is removed using hair removal and scalp is disinfected. Then, bupivicaine nerve block is injected once under the scalp. The scalp is removed with surgical scissors. The skull is cleaned and dried with 3% hydrogen peroxide, followed by application of the sterile dental adhesive Optibond (Kerr Dental; cured with blue light). A < 0.2 mm burr hole is dug above the right cerebellum for a ground wire. A stainless-steel wire is inserted into the burr hole between the skull and the brain, parallel to the brain surface, then the wire is affixed to the skull with sterile dental acrylic. This stainless-steel wire is connected to the ground of system. A titanium headplate (2 cm long, ~1 g) is positioned above lambda. Then, the plate is positioned parallel to skull and permanently fixed in place with sterile dental acrylic. All protocols and experiments were approved by the Virginia Tech (Blacksburg, VA, USA) Institutional Animal Care and Use Committee (IACUC).

4.6. Microdrive implantation

The Tetro-DOpE probes epoxied onto the 3-printed plate were attached to custom metal microdrives (Vöröslakos et al., 2021) prior to implantation. Surgical procedures for headbar implantation (see above) are followed, with a deviation following the ground wire implantation. A linear burr hole, (using dental drill with 0.2 mm burr bit) just larger than the probes, is dug above the hippocampus. The microdrive and probe, held by the stereotax, is lowered into the craniotomy 1 mm, until the probe is in the cortex just above the hippocampus. The base of the microdrive is then permanently fixed to the skull with sterile dental acrylic. A miniature faraday cage is then constructed and fixed to the skull of the mouse to minimize noise, and the ground wire is attached to the faraday cage. The entire implant is wrapped in vetwrap bandaging tape to protect the animal and implant from damage. Following recovery, the probe is slowly lowered using the microdrive while recording online to identify electrophysiological markers of the hippocampus and neurons. Following each movement of the probe, location is confirmed 24 h later after tissue relaxes.

4.7. AAV injection

Mice, mounted in the stereotax, are induced and maintained at a surgical plane of anesthesia with isoflurane. Hair is removed using hair removal and scalp is disinfected. Then, bupivicaine nerve block is injected once under the scalp. A < 0.2 mm burr hole is dug above the hippocampus (mm from bregma: −1.8, lateral: 1.5). Glass pipette containing AAV5-CaMKIIa-hChR2(H134R)-EYFP (UNC Gene Therapy Center – Vector Core) is lowered into CA1 (mm from surface: 1.2) at a slow rate. 100 nL of AAV (titer: 4.1×10^{12} GC/mL) is injected into tissue at a rate of 1 nLs^{-1} using microinjector syringe pump (WPI: MICRO2T & 504127). Glass pipette is kept in place for 5 min for virus to diffuse, then slowly removed from brain. Craniotomy is covered using biocompatible silicon elastomer (Kwik-SIL; World Precision Instruments). Then, the scalp is closed with Vetbond (3M).

4.8. Craniotomy

Mice, mounted in the stereotax, are induced and maintained at a surgical plane of anesthesia with isoflurane. A 0.5–1.0 mm burr hole (using dental drill with 0.2 mm burr bit) is dug above the hippocampus. Then, the dura is removed. Biocompatible silicon elastomer (Kwik-cast; World Precision Instruments) is applied to the burr hole to keep the brain from drying.

4.9. In-vivo recording

Mice, habituated to head-fixed navigation, are placed in the head fixation apparatus, and the Tetro-DOpE probe is lowered through the craniotomy into the brain. When SPW-Rs are recognized, the probe is left in place for 30–45 min until tissue is relaxed. The amplified neural signals are then recorded with RHD2000 system (Intan Technologies LLC). For freely moving chronic mouse recordings, the omnetic connector from the PCB was connected to RHD2000 system and the electrophysiology signal was recorded.

4.10. Optical stimulation

The optical ferrule from the probe is coupled to a diode-pumped solid-state (DPSS) laser (Laserglow Technologies, 100 mW maximum power, wavelength = 473 nm) through a mating sleeve (Thorlabs). The optical output is calibrated each optical stimulation session. The optically evoked LFP activity is closely monitored to determine power output necessary to optically induce SPW-Rs. Across experiments optical power varied between 6 and 92 μW and optical power density to be 3.1–47.3 mW/mm^2.

4.11. Immunohistochemistry

Animals were implanted with a stainless-steel probe or a fiber probe for 2 weeks and then anesthetized with a ketamine (20 mg/mL)/xylazine (2 mg/mL) solution and transcardially perfused with PBS (Fisher BP661–10) followed by 4% paraformaldehyde (PFA) (Electron Microscopy Sciences Cat. #15714-S) in PBS. Upon extraction, the brain was kept in 4% PFA overnight at 4 °C and then placed into PBS containing 0.02% sodium azide (sigma S8032) and serially sectioned into 50 μm transverse slices on a Leica VT 1000S vibratome. All slices were blocked for 2 h at room temperature in the blocking solution that contained 10% goat serum (Millipore S26-100 ML) and 0.03%Triton X-100 (Sigma T9284) in PBS. After blocking, slices were incubated with primary antibodies diluted in blocking solution diluted 1:3 in PBS overnight at 4 °C. Primary antibodies used included chicken anti-GFAP (abcam Cat. #ab4674, 1:500), guinea pig anti-NeuN (Synaptic Systems. #266004, 1:500), and rabbit anti-Iba1 (Wako Cat. #019–19741, 1:500). Following primary incubation, slices were washed six times with PBS for 10 min at room temperature with agitation. Secondary antibodies diluted in blocking solution diluted 1:3 in PBS were added at 4 °C overnight. Secondary antibodies used included goat anti-chicken Alexa Fluor 647 (Jackson ImmunoResearch Cat. #103-605-155, 1:500) goat anti-guinea pig Alexa Fluor 488 (Jackson ImmunoResearch Cat. #106-545-003, 1:500) and goat anti-rabbit Alexa Fluor 555 (abcam Cat. # ab150078, 1:500). Slices were then washed six times with PBS for 10 min at room temperature with agitation. Slices were mounted on glass slides with ProLong Antifade Mounting Medium with DAPI (ThermoFisher Cat. #P36931). Optical sections were acquired using a Leica Stellaris 8 laser scanning microscope using a HC PL APO 20X/N.A.0.75 air objective. Data was quantified using Imaris 10.1 (Oxford Instruments Group). Neuron density was determined utilizing the spot detection feature in Imaris. For volume analysis and quantification of IBA1 and GFAP labeled cells within the volumetric confocal dataset, 3D reconstructions were created using Imaris's Surface creation feature. All statistical analyses were conducted using Prism version 10.2.3 (GraphPad).

4.12. Data analysis

Data analysis was performed in Matlab (The Mathworks). Kilosort, spike2, and Matlab custom scripts were written to sort neural spikes and analyze the local field potentials. The extracellular electrophysiology signals were digitally filtered from 0.5 to 500 Hz and 300–8000 Hz to obtain local field potentials and single unit traces respectively. The spike sorting algorithm was implemented by first filtering out individual spikes using standard deviation dependent threshold. Then, the dimensionality of the spikes were reduced via principal component analysis and individual clusters were identified with K-means clustering.

Code availability

The MATLAB scripts for analysis are available from upon request.

CRediT authorship contribution statement

Jongwoon Kim: Writing – review & editing, Writing – original draft, Visualization, Validation, Software, Methodology, Investigation, Formal analysis, Data curation, Conceptualization. **Earl Gilbert:** Validation, Methodology. **Kaiser Arndt:** Validation, Software. **Hengji Huang:** Methodology. **Patrycja Oleniacz:** Investigation. **Shan Jiang:** Investigation. **Ian Kimbrough:** Investigation. **Harald Sontheimer:** Validation. **Daniel Fine English:** Writing – review & editing, Visualization, Validation, Supervision, Methodology, Formal analysis, Data curation. **Xiaoting Jia:** Writing – review & editing, Writing – original draft, Visualization, Validation, Supervision, Investigation, Funding acquisition, Conceptualization.

Declaration of competing interest

The authors declare the following financial interests/personal relationships which may be considered as potential competing interests: Xiaoting Jia reports financial support was provided by National Science Foundation. Xiaoting Jia reports financial support was provided by National Institutes of Health. If there are other authors, they declare that they have no known competing financial interests or personal relationships that could have appeared to influence the work reported in this paper.

Data availability

Data will be made available on request.

Acknowledgement

X.J. gratefully acknowledges funding support from the National Institute of Health (R01NS123069, R21EY033080, R56AG077720) and National Science Foundation (ECCS-1847436). DFE gratefully acknowledges funding support from The Simons Foundation and The Whitehall Foundation.

Appendix A. Supplementary data

Supplementary data to this article can be found online at https://doi.org/10.1016/j.bios.2024.116696.

References

Ahmed, R., Reifsnider, K., 2011. Study of influence of electrode geometry on impedance spectroscopy. Int. J. Electrochem. Sci. 6, 1159–1174.
Bruce, C., Desimone, R., Gross, C.G., 1981. Visual properties of neurons in a polysensory area in superior temporal sulcus of the macaque. J. Neurophysiol. 46, 369–384.
Buzsáki, G., 2004. Large-scale recording of neuronal ensembles. Nat. Neurosci. 7, 446–451.
Buzsáki, G., 2015a. Hippocampal sharp wave-ripple: a cognitive biomarker for episodic memory and planning. Hippocampus 25, 1073–1188.
Buzsáki, G., 2015b. Hippocampal sharp wave-ripple: a cognitive biomarker for episodic memory and planning. Hippocampus 25, 1073–1188.
Buzsáki, G., Draguhn, A., 2004. Neuronal oscillations in cortical networks. Science 304, 1926–1929.
Buzsáki, G., Lai-Wo, S.L., Vanderwolf, C.H., 1983. Cellular bases of hippocampal EEG in the behaving rat. Brain Res. Rev. 6, 139–171.
Canales, A., et al., 2015. Multifunctional fibers for simultaneous optical, electrical and chemical interrogation of neural circuits in vivo. Nat. Biotechnol. 33, 277–284.
Carandini, M., 2012. From circuits to behavior: a bridge too far? Nat. Neurosci. 15, 507–509.

Chen, W., et al., 2022. The roles of optogenetics and technology in neurobiology: a review. Front. Aging Neurosci. 14.
Deisseroth, K., 2015. Optogenetics: 10 years of microbial opsins in neuroscience. Nat. Neurosci. 18, 1213–1225.
Ekstrom, A.D., et al., 2003. Cellular networks underlying human spatial navigation. Nature 425, 184–188.
Emiliani, V., et al., 2022. Optogenetics for light control of biological systems. Nat. Rev. Meth. Primers 2, 55.
Eunah, K., Mihály, V., György, B., Euisik, Y., 2022. flexLiTE: flexible micro-LED integrated optoelectrodes for minimally-invasive chronic deep-brain study. bioRxiv 2022, 503006, 2008.2005.
Fenno, L., Yizhar, O., Deisseroth, K., 2011. The development and application of optogenetics. Annu. Rev. Neurosci. 34, 389–412.
Fernández-Ruiz, A., et al., 2019. Long-duration hippocampal sharp wave ripples improve memory. Science 364, 1082–1086.
Garwood, I.C. et al. Multifunctional fibers enable modulation of cortical and deep brain activity during cognitive behavior in macaques. Sci. Adv. 9, eadh0974.
Gray, C.M., Maldonado, P.E., Wilson, M., McNaughton, B., 1995. Tetrodes markedly improve the reliability and yield of multiple single-unit isolation from multi-unit recordings in cat striate cortex. J. Neurosci. Methods 63, 43–54.
Hafting, T., Fyhn, M., Molden, S., Moser, M.-B., Moser, E.I., 2005. Microstructure of a spatial map in the entorhinal cortex. Nature 436, 801–806.
Hong, G., Lieber, C.M., 2019. Novel electrode technologies for neural recordings. Nat. Rev. Neurosci. 20, 330–345.
Jeong, J.-W., et al., 2015. Wireless optofluidic systems for programmable In Vivo pharmacology and optogenetics. Cell 162, 662–674.
Jiang, S., et al., 2020. Spatially expandable fiber-based probes as a multifunctional deep brain interface. Nat. Commun. 11, 6115.
Joshi, J., Rubart, M., Zhu, W., 2020. Optogenetics: background, methodological advances and potential applications for cardiovascular research and medicine. Front. Bioeng. Biotechnol. 7.
Kim, K., et al., 2020. Artifact-free and high-temporal-resolution in vivo opto-electrophysiology with microLED optoelectrodes. Nat. Commun. 11, 2063.
Kim, J., et al., 2024. T-DOpE probes reveal sensitivity of hippocampal oscillations to cannabinoids in behaving mice. Nat. Commun. 15, 1686.
Kovács, K.A., et al., 2016. Optogenetically blocking sharp wave ripple events in sleep does not interfere with the formation of stable spatial representation in the CA1 area of the Hippocampus. PLoS One 11, e0164675.
Liu, A.A., et al., 2022. A consensus statement on detection of hippocampal sharp wave ripples and differentiation from other fast oscillations. Nat. Commun. 13, 6000.
Mokri, Y., et al., 2017. Sorting overlapping spike waveforms from electrode and tetrode recordings. Front. Neuroinf. 11.
Neto, J.P., et al., 2018. Does impedance matter when recording spikes with polytrodes? Front. Neurosci. 12.
O'Keefe, J., Dostrovsky, J., 1971. The hippocampus as a spatial map. Preliminary evidence from unit activity in the freely-moving rat. Brain Res. 34, 171–175.
Ouyang, W., et al., 2023. A wireless and battery-less implant for multimodal closed-loop neuromodulation in small animals. Nat. Biomed. Eng. 7, 1252–1269.
Ovechkina, V.S., Zakian, S.M., Medvedev, S.P., Valetdinova, K.R., 2021. Genetically encoded fluorescent biosensors for biomedical applications. Biomedicines 9.
Park, S., et al., 2017. One-step optogenetics with multifunctional flexible polymer fibers. Nat. Neurosci. 20, 612–619.
Rein, M., et al., 2018. Diode fibres for fabric-based optical communications. Nature 560, 214–218.
Rubehn, B., Wolff, S.B., Tovote, P., Lüthi, A., Stieglitz, T., 2013. A polymer-based neural microimplant for optogenetic applications: design and first in vivo study. Lab Chip 13, 579–588.
Rubin, A., et al., 2019. Revealing neural correlates of behavior without behavioral measurements. Nat. Commun. 10, 4745.
Sahasrabudhe, A., et al., 2023. Multifunctional microelectronic fibers enable wireless modulation of gut and brain neural circuits. Nat. Biotechnol. 42, 892–904.
Schultz, W., 1986. Responses of midbrain dopamine neurons to behavioral trigger stimuli in the monkey. J. Neurophysiol. 56, 1439–1461.
Shin, H., et al., 2015. Neural probes with multi-drug delivery capability. Lab Chip 15, 3730–3737.
Shin, H., et al., 2019. Multifunctional multi-shank neural probe for investigating and modulating long-range neural circuits in vivo. Nat. Commun. 10, 3777.
Stark, E., et al., 2014. Pyramidal cell-interneuron interactions underlie hippocampal ripple oscillations. Neuron 83, 467–480.
Vöröslakos, M., Petersen, P.C., Vöröslakos, B., Buzsáki, G., 2021. Metal microdrive and head cap system for silicon probe recovery in freely moving rodent. Elife 10, e65859.
Vöröslakos, M., et al., 2022. HectoSTAR μLED optoelectrodes for large-scale, high-precision in vivo opto-electrophysiology. Adv. Sci. 9, 2105414.
Wang, X.-J., 2010. Neurophysiological and computational principles of cortical rhythms in cognition. Physiol. Rev. 90, 1195–1268.
Wang, M., Da, Y., Tian, Y., 2023. Fluorescent proteins and genetically encoded biosensors. Chem. Soc. Rev. 52, 1189–1214.
Wilson, M.A., McNaughton, B.L., 1994. Reactivation of hippocampal ensemble memories during sleep. Science 265, 676–679.
Yoon, Y., et al., 2022. Neural probe system for behavioral neuropharmacology by bi-directional wireless drug delivery and electrophysiology in socially interacting mice. Nat. Commun. 13, 5521.
Yuste, R., MacLean, J.N., Smith, J., Lansner, A., 2005. The cortex as a central pattern generator. Nat. Rev. Neurosci. 6, 477–483.
Zhang, Y., et al., 2021. Cholinergic suppression of hippocampal sharp-wave ripples impairs working memory. Proc. Natl. Acad. Sci. USA 118, e2016432118.
Zhao, Z., et al., 2017. Nanoelectronic coating enabled versatile multifunctional neural probes. Nano Lett. 17, 4588–4595.
Zheng, N., et al., 2023. Multifunctional fiber-based optoacoustic emitter as a bidirectional brain interface. Adv. Healthcare Mater. 12, 2300430.
Zhou, Y., et al., 2022. A silk-based self-adaptive flexible opto-electro neural probe. Microsyst. Nanoeng. 8, 118.
Zou, L., et al., 2021. Self-assembled multifunctional neural probes for precise integration of optogenetics and electrophysiology. Nat. Commun. 12, 5871.
Zutshi, I., Buzsáki, G., 2023. Hippocampal sharp-wave ripples and their spike assembly content are regulated by the medial entorhinal cortex. Curr. Biol. 33, 3648–3659. e3644.